A&A 521, L13 (2010)
DOI: 10.1051/0004-6361/201015095

Astronomy & Astrophysics
Special feature

Herschel/HIFI: first science highlights

Letter to the Editor

Excitation and abundance of C_3 in star forming cores

Herschel/HIFI⋆ observations of the sight-lines to W31C and W49N⋆⋆

B. Mookerjea[1], T. Giesen[2], J. Stutzki[2], J. Cernicharo[3], J. R. Goicoechea[3], M. De Luca[4], T. A. Bell[5], H. Gupta[6], M. Gerin[4], C. M. Persson[7], P. Sonnentrucker[9], Z. Makai[2], J. Black[7], F. Boulanger[10], A. Coutens[13], E. Dartois[10], P. Encrenaz[4], E. Falgarone[4], T. Geballe[14], B. Godard[4], P. F. Goldsmith[6], C. Gry[11], P. Hennebelle[4], E. Herbst[8], P. Hily-Blant[12], C. Joblin[13], M. Kaźmierczak[17], R. Kołos[16], J. Krełowski[17], D. C. Lis[5], J. Martin-Pintado[3], K. M. Menten[15], R. Monje[5], J. C. Pearson[6], M. Perault[4], T. G. Phillips[5], R. Plume[18], M. Salez[4], S. Schlemmer[2], M. Schmidt[19], D. Teyssier[20], C. Vastel[13], S. Yu[4], P. Dieleman[23], R. Güsten[15], C. E. Honingh[2], P. Morris[21], P. Roelfsema[23], R. Schieder[2], A. G. G. M. Tielens[22], and J. Zmuidzinas[5]

(Affiliations are available on page 5 of the online edition)

Received 31 May 2010 / Accepted 2 July 2010

ABSTRACT

We present spectrally resolved observations of triatomic carbon (C_3) in several ro-vibrational transitions between the vibrational ground state and the low-energy ν_2 bending mode at frequencies between 1654−1897 GHz along the sight-lines to the submillimeter continuum sources W31C and W49N, using *Herschel*'s HIFI instrument. We detect C_3 in absorption arising from the warm envelope surrounding the hot core, as indicated by the velocity peak position and shape of the line profile. The sensitivity does not allow to detect C_3 absorption due to diffuse foreground clouds. From the column densities of the rotational levels in the vibrational ground state probed by the absorption we derive a rotation temperature ($T_{\rm rot}$) of ∼50−70 K, which is a good measure of the kinetic temperature of the absorbing gas, as radiative transitions within the vibrational ground state are forbidden. It is also in good agreement with the dust temperatures for W31C and W49N. Applying the partition function correction based on the derived $T_{\rm rot}$, we get column densities $N(C_3) \sim 7{-}9 \times 10^{14}$ cm^{-2} and abundance $x(C_3) \sim 10^{-8}$ with respect to H_2. For W31C, using a radiative transfer model including far-infrared pumping by the dust continuum and a temperature gradient within the source along the line of sight we find that a model with $x(C_3) = 10^{-8}$, $T_{\rm kin} = 30{-}50$ K, $N(C_3) = 1.5 \times 10^{15}$ cm^{-2} fits the observations reasonably well and provides parameters in very good agreement with the simple excitation analysis.

Key words. ISM: lines and bands – ISM: molecules – radiative transfer – ISM: individual objects: W49N – ISM: individual objects: W31C

1. Introduction

Small carbon chains are relevant in the chemistry of stellar and interstellar environments for several reasons: ubiquitous interstellar spatial distribution, they likely participate in the formation of long carbon chain molecules, and they are products in photo-fragmentation processes of larger species such as PAHs. Triatomic carbon, C_3, was first tentatively identified in interstellar gas by Van Orden et al. (1995) and Haffner & Meyer (1995). The mid-infrared spectrum of C_3 (ν_3 antisymmetric stretching mode) was measured in the circumstellar envelope of CW Leo (IRC +10216) by Hinkle et al. (1988), and in low-resolution interstellar absorption in the far-IR (ν_2 bending mode) toward Sgr B2 by Cernicharo et al. (2000). Giesen et al. (2001) discussed new laboratory data on the vibrational spectrum of C_3 in its low-frequency bending mode and re-visited the first identification of the ν_2 $R(2)$ line in absorption toward Sgr B2 (Van Orden et al. 1995). The abundance and excitation of C_3 in translucent clouds were determined convincingly by Maier et al. (2001), Roueff et al. (2002) and Oka et al. (2003) at optical wavelengths.

The Heterodyne Instrument for the Far-Infrared (HIFI; de Graauw et al. 2010) on board the *Herschel* Space Observatory (Pilbratt et al. 2010), with its broad frequency coverage, high sensitivity and spectral resolution provides for the first time the opportunity for a systematic study of carbon chain molecules such as C_3 through probing several ro-vibrational lines at full spectral resolution. In this letter, we present the first results of our search for C_3 obtained from observations of the sight-lines to the bright far-infrared (FIR) continuum sources W31C and W49N as part of the PRISMAS ("PRobing InterStellar Molecules with Absorption line Studies") key program (Gerin et al. 2010).

W31C (G10.6 − 0.4) is one of three bright HII regions within the W31 complex, and an extremely luminous submillimeter and infrared continuum source ($L_{\rm IR} \sim 10^7\ L_\odot$ Wright et al. 1977). Located at a distance of $4.8^{+0.4}_{-0.8}$ kpc (Fish et al. 2003) with $v_{\rm LSR} = -3$ to -1 km s^{-1} (Miettinen et al. 2006), the sight-line to G10.6 − 0.4 intersects several foreground molecular clouds (Corbel & Eikenberry 2004). W49N is one of the three main IR peaks of W49A, which has a luminosity of ($L_{\rm bol} \sim 10^7\ L_\odot$ Ward-Thompson & Robson 1990). It is located at a distance of

⋆ Appendix A (page 5) is only available in electronic form at http://www.aanda.org

⋆⋆ *Herschel* is an ESA space observatory with science instruments provided by European-led Principal Investigator consortia and with important participation from NASA.

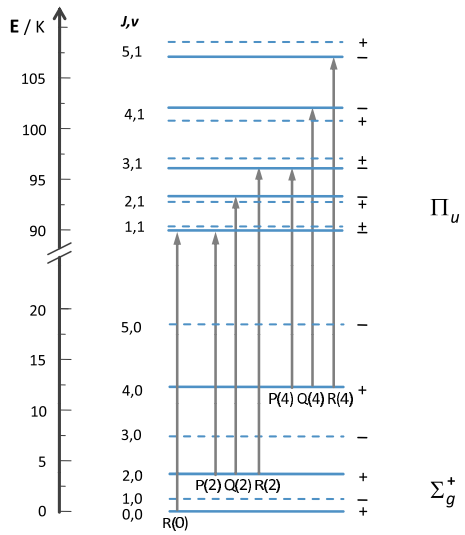

Fig. 1. Energy level diagram of Σ_g^+ ground state and Π_u lowest bending mode state of C_3. Due to nuclear spin statistics half of the rotational energy levels (dashed lines) are missing. Allowed ro-vibrational *P*-, *Q*-, and *R*-branch transitions from $v = 0$ to $v' = 1$ follow $- \leftarrow +$ selection rules.

11.4 kpc and has $v_{LSR} = 12$ km s^{-1}. The sight-line toward W49N is spectroscopically interesting because of the numerous features contributed by W49A itself, as well as by additional clouds associated with the Sagittarius spiral arm (which crosses the line of sight twice). Numerous spectroscopic studies (both emission and absorption) have been carried out in the past towards both these sources (e.g., Plume et al. 2004; Neufeld et al. 2010).

2. C_3 energy level diagram and radiative transitions

Linear C_3 has an energetically unusually low ν_2 bending mode at only ~90 K. Ro-vibrational transitions of the ν_2 band in its $^1\Sigma_g^+$ electronic ground state have been reported by Gendriesch et al. (2003) and Schmuttenmaer et al. (1990). $P(J)$ transitions with $J = 2, 4, 6$, $R(J)$ with $J = 0, 2, 4, 6$, and $Q(J)$ with $J = 2, 4, \ldots$ 16 have been measured in the laboratory, using high resolution Terahertz sideband spectrometers at Berkeley (Schmuttenmaer et al. 1990) and Cologne (Gendriesch et al. 2003) with frequency accuracies of 7 MHz and 0.5 MHz respectively, which corresponds to line frequency uncertainties of 1.1 km s^{-1} and 0.08 km s^{-1}. All data were used in a global fit analysis to obtain most accurate molecular constants (Giesen et al. 2001) which are presented as line lists for astronomical observations in the Cologne Data Base for Molecular Spectroscopy (CDMS) (Müller et al. 2005). The ground state of C_3 has $^1\Sigma_g^+$ symmetry while the vibrational excited ν_2 is a two-fold degenerate bending state of Π_u symmetry. Due to the ^{12}C nuclear spin of $I = 0$ in the ground state only levels of (+) parity are present, while for the excited bending state only levels with (−) parity are allowed. As a consequence, in the ground state of C_3 all odd numbered J rotational levels are missing, whereas in the vibrational excited Π_u state both, even and odd J rotational levels are present, but the two-fold degeneracy of the vibrational state is lifted (see Fig. 1). Consequently, the statistical weights of the ro-vibrational levels is simply given by the rotational degeneracy: $g_{J,v} = 2J + 1$. The ν_2 bending mode has a perpendicular type spectrum with a calculated vibrational dipole moment of 0.437 Debye (Jensen et al. 1992) which shows prominent *Q*-, *P*-, and *R*-branch transitions.

Table 1. Spectroscopic parameters for the observed C_3 transitions.

Name	Transition $(J', v')\leftarrow(J, v)$	Frequency[a] [MHz]	A-coeff 10^{-3} s^{-1}	E_l [K]
$P(10)$	(9, 1)←(10, 0)	1654081.66(4.68)[b]	2.38	47.3
$P(4)$	(3, 1)←(4, 0)	1787890.57(6.90)	2.72	8.6
$Q(2)$	(2, 1)←(2, 0)	1890558.06(0.25)	7.51	2.6
$Q(4)$	(4, 1)←(4, 0)	1896706.56(0.15)	7.58	8.6

Notes. [(a)] Experimental rest frequencies, uncertainties are given in parentheses; [(b)] calculated frequency and 1σ uncertainty taken from CDMS catalog.

For the analysis of the HIFI C_3 data, rest frequencies for $P(4)$, $Q(2)$, and $Q(4)$ were taken from laboratory measurements while for $P(10)$ the rest frequency has been obtained from a global fit of all available laboratory data.

3. Observations and data reduction

Along the sight-lines to W31C and W49N we have observed four lines of the ν_2 bending mode, $P(4)$, $Q(2)$, $Q(4)$ and $P(10)$ (the latter only in W31C), of triatomic carbon in the upper sideband of the HIFI bands 7a, 7b and the lower sideband of band 6b of the HIFI receiver. The observations of W31C and W49N were carried out on 2010 March 8 and 2010 April 19 respectively. The $P(10)$ line was available as a "bonus" for an LO tuning dedicated to observe the CH line at 1661 GHz and it is yet to be observed in W49N with HIFI. All observations are in dual beam switch (DBS) mode and with the wide band spectrometer with its spectral resolution of 1.1 MHz, corresponding to a velocity resolution of ~0.17 km s^{-1} at the frequencies of the C_3 lines. To identify the line origin from the lower and upper sidebands, each line was observed with three LO settings shifted by 15 km s^{-1} relative to each other. The $Q(2)$ line also shows up in the $Q(4)$ observations from the lower sideband, and, for one of the LO tunings, partially overlap with the former. The data were first processed with HIPE (Ott et al. 2010), and subsequently exported to CLASS. At the high frequencies for these observations the H and V polarizations were at times found to be discrepant in the measured continuum level. Observations optimized for reliable continuum measurement were used to select the spectra with the correct continuum level, used for the subsequent analysis. All spectra were smoothed to a resolution of ~0.68 km s^{-1} and the rms noise level for the spectra lie between 0.01−0.03 K. Table 2 gives the measured double sideband continuum level (T_c). For the remainder of the paper we discuss the line intensities normalized to the single-sideband continuum level, where we have assumed a sideband gain ratio of unity.

4. Results

We have for the first time detected the spectrally resolved ν_2 band transitions $P(4)$, $P(10)$, $Q(2)$ and $Q(4)$ lines of C_3. Figure 2 shows the observed spectra normalized to the (single sideband) continuum level. A multi-component Gaussian with common velocity width and spacing and individual amplitudes for each line was fitted to derive the basic parameters of the absorption spectra. Table 2 presents the fit results and their uncertainties. The $P(10)$ spectrum is affected by the spectral lines of CH (1661.10726 GHz) and H_2O (1661.007637 GHz) from the upper sideband.

The C_3 absorption features towards W31C and W49N are centered near 0 km s^{-1} and 11 km s^{-1} respectively. The systemic velocities of W31C and W49N are at $v_{LSR} = -1$ km s^{-1} and

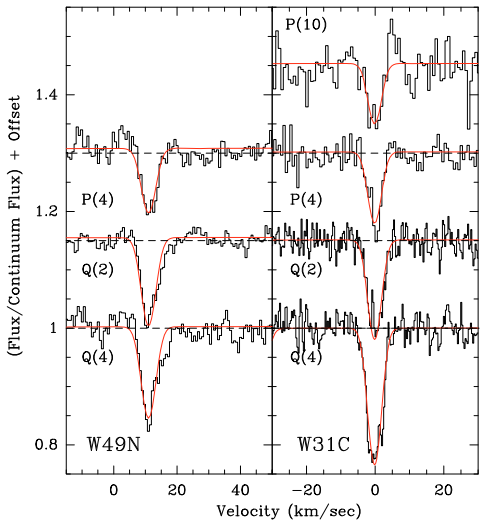

Fig. 2. The observed absorption spectra of the $P(4)$, $P(10)$, $Q(2)$ and $Q(4)$ ro-vibrational transitions of C_3 towards W49N (*left*) panel and W31C (*right panel*), plotted along with the best-fit profiles obtained by simultaneous Gaussian fitting to all lines.

Table 2. Parameters derived from simultaneous Gaussian fitting to all the line profiles and column densities estimated from the fitted intensities.

Transition	W31C			W49N		
	T_c [K]	$\int \tau dv$ [km/s]	N_l [cm^{-2}]	T_c [K]	$\int \tau dv$ [km s^{-1}]	N_l [cm^{-2}]
$P(10)$	11.4 ± 0.4	0.51	1.0×10^{14}	...	.....	
$P(4)$	10.5 ± 0.3	0.61	1.5×10^{14}	16.8 ± 0.2	0.62	1.6×10^{14}
$Q(2)$	11.8 ± 0.2	0.87	7.2×10^{13}	18.3 ± 0.3	0.87	7.3×10^{13}
$Q(4)$	11.8 ± 0.2	1.22	1.0×10^{14}	18.3 ± 0.2	0.90	7.6×10^{13}

Notes. The fitted values of line center and linewidth are: for W31C $V_{cen} = -0.09 \pm 0.06$ km s^{-1} and $\Delta V = 4.5 \pm 0.1$ km s^{-1} and for W49N $V_{cen} = 11.0 \pm 0.1$ km s^{-1}, and $\Delta V = 5.3 \pm 0.2$ km s^{-1}.

12 km s^{-1}. Thus the C_3 absorption lines detected here appear to be physically associated with the hot core itself and most likely arise in the lower density warm envelope surrounding them. We do not detect any absorption feature arising from the foreground clouds towards either of these sources (see Sect. 5).

4.1. Two-layer excitation analysis

We first consider a simple two-layer model in which a (warm) absorbing layer without continuum opacity lies in front of a (hotter) emitting background source. We used the formalism explained in detail in Appendix A to obtain estimates of the rotational temperature (T_{rot}) from the state specific column densities (Table 2). The $J = 4$ column densities are redundantly determined through both the $P(4)$ and $Q(4)$ transitions. One of the primary sources of error in determination of the state specific column densities is the determination of the continuum levels. We estimate the uncertainty in the derived column densities to be 20%. For both W31C and W49N the discrepancy in the $J = 4$ column densities determined from $P(4)$ and $Q(4)$ is much larger than this uncertainty. We can only speculate on the reason: firstly, the assumptions of the simple two-layer model may not be appropriate and a more sophisticated model should be used (see below). Secondly, we note that in case the C_3 absorption fills only a fraction of the solid angle of the continuum source within the beam, the intrinsic absorption would be much larger, possibly reaching saturation for the stronger $Q(4)$ line. We use

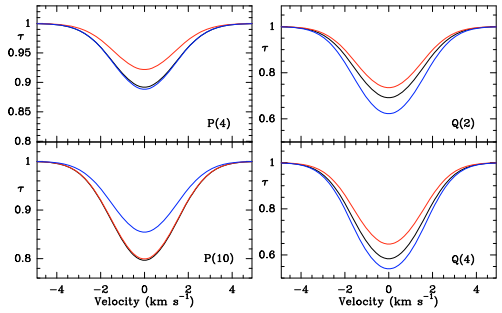

Fig. 3. Model predictions for the $Q(2)$, $Q(4)$, $P(2)$ and $P(10)$ lines of the $\nu_2 = 1-0$ transition of C_3 in W31C. The black lines correspond to a model with $n(H_2) = 10^5$ cm^{-3}, $x(C_3) = 5 \times 10^{-8}$ and $T_{kin} = 50$ K. The red lines correspond to a model with $n(H_2) = 5 \times 10^5$ cm^{-3}, $x(C_3) = 10^{-8}$ and $T_{kin} = 50$ K. Finally, the blue lines correspond to the same parameters as the red ones except that $T_{kin} = 30$ K.

an average of the column densities at $J = 4$ obtained from $P(4)$ and $Q(4)$ for the rest of the paper.

Using the formulae from Appendix A, we obtain for W49N a T_{rot} of 70 K with a large formal error. This is consistent with T_{dust} derived from dust continuum observations as 43 K (Vastel et al. 2000) since T_{gas} can be higher than T_{dust} through direct gas heating near the core. For $T_{rot} = 70$ K we calculate from the $J = 2$ column density a total column density of $N(C_3) = 9 \times 10^{14}$ cm^{-2}.

For W31C we have used the state-specific column densities (N_J) at $J = 2$, 4 and 10, to determine T_{rot} and $N(C_3)$ from the slope and the intercept respectively of a linear fit to the $\log(\frac{N_J}{2J+1})$ vs. E_J points ("rotation diagram"). Assuming a uniform 20% error in the determination of the column densities we obtain $T_{rot} = 56 \pm 6$ K and $N(C_3) = (7 \pm 0.5) \times 10^{14}$ cm^{-2}. The estimated T_{rot} is consistent with the observed dust temperature of 52 K derived from continuum observations by Mueller et al. (2002).

4.2. Radiative transfer models for C_3 excitation in W31C

In the likely scenario that the dust continuum source and its associated continuum opacity are coexistent with the gas that absorbs in the C_3 lines, the C_3 molecule will be embedded in a relatively strong continuum radiation which would contribute to the ro-vibrational excitation. In addition, the source intrinsic continuum will partially fill in the line absorption. Thus, in a more detailed approach we use a radiative transfer model, which considers FIR pumping by the dust continuum (Cernicharo et al. 2000) and a temperature gradient of the continuum source along the line of sight. For W31C we find that the C_3 column densities can be interpreted by a cloud which is twice the size of the continuum source, has a molecular hydrogen density $n(H_2) = 10^5$ cm^{-3}, $v_{turb} = 2$ km s^{-1}, abundance $x(C_3) = 5 \times 10^{-8}$, kinetic temperature of 50 K and $N(C_3) = 1.5 \times 10^{15}$ cm^{-2} (see Fig. 3). The fact that the C_3 column density comes out larger in this more detailed model is expected, as the dust opacity partially fills-in the absorption line.

The main source of uncertainty in these models are the ro-vibrational collisional rates which are based on rather crude assumptions (Cernicharo et al. 2000). However, irrespective of the adopted collisional rates the ground state is always thermalized, even in the presence of a strong IR radiation field in our models. We find that owing to the lack of a permanent electrical dipole moment the uncertainties in the collisional rates have little effect on the emerging intensities. Figure 3 also shows that the

resulting absorption depths are almost unaffected by a change in the local density (and hence abundance) by as much as a factor of 5, as long as the column density remains constant. We find that the $\nu_2 = 1-0$ transitions are dominated by infrared pumping. The ro-vibrational excitation temperature in the inner part of the cloud is 35−37 K for the lowest rotational levels and around 20 for the higher-J states. In the external layers T_{ex} decreases by 20 and 10 K, respectively. In a second model with $n(H_2) = 5 \times 10^5$ cm^{-3} and $x(C_3) = 10^{-8}$ the results are almost equally consistent with the observations. We also note, that depending on the geometrical arrangement, the FIR-pumping in the ro-vibrational transitions can result in the net effect of lowering the rotational temperature in the vibrational ground state slightly below the kinetic temperature of the gas.

We find that the major effect on the resulting absorption depths is related to the kinetic temperature adopted for the absorbing gas. In Fig. 3 the blue lines correspond to a gas with $T_{kin} = 30$ K. The high-J lines of the ground state are less populated than in the previous case and the opacities for the $\nu_2 = 1-0$ transitions decrease. If the opacity of the ro-vibrational lines become larger than 1, and the central continuum source is optically thick at the wavelengths of the $\nu_2 = 1-0$ transitions, then the ν_2 level becomes thermalized to the temperature of the dust. This effect can be counterbalanced by decreasing the gas temperature in the external layers of the cloud. Clearly, a more elaborate analysis than can be presented in this letter, is needed to explore the full parameter range.

5. Discussion

In the absence of allowed radiative transitions in the ground state, the excitation of C_3 in the $\nu_2 = 0$ state can be assumed to be thermalized to the kinetic temperature: $T_{rot} = T_{kin}$. However, T_{rot} can be larger than T_{dust} in the presence of direct gas heating mechanism like the photoelectric heating. The ν_2 mode on the other hand could be excited by collisions and as well as by infrared photons. With Einstein coefficients ranging between 2 and 7×10^{-3} s^{-1}, the line opacities can be high and the infrared pumping rather efficient. As a result, the excitation temperatures of the ro-vibrational lines are much lower, typically between the beam-diluted T_{dust} and T_{kin} and hence the lines are seen in absorption. However, as explained above, the excitation temperature within the rotation ladder of the ground vibrational state can have values larger than T_{dust}.

Crude estimates based on the "two-layer" approach derive a T_{rot} consistent with the dust temperature of the continuum source and give column densities of C_3 in W31C and W49N to be between $7-9 \times 10^{14}$ cm^{-2}. Using the more elaborate radiative transfer model we derived a column density of 1.5×10^{15} cm^{-2} for W31C for T_{kin} of 30 K. Based on the discussion above we further argue that the thus derived column density of C_3 is likely to be a lower limit. Implicit assumptions like a source filling factor of unity, $T_{ex} \ll T_c$ etc. in the two-layer approach translate to an underestimate of T_{rot}. Moreover the source intrinsic continuum opacity at 1.9 THz partially re-fills the absorption (as shown in the radiative transfer model), and hence the column densities derived from the radiative transfer model are higher than those derived in the two-layer model. Thus taking all uncertainties into account we conclude that for both W31C and W49N the C_3 column densities are $\sim 10^{15}$ cm^{-2}, correct to within a factor of 2 or so. The H_2 column densities in W31C and W49N are 9.2×10^{22} cm^{-2} (Miettinen et al. 2006) and $\sim 10^{23}$ cm^{-2} respectively, so that the abundances of C_3 are $\sim 10^{-8}$. It is interesting to note that warm-up chemical models of the environment around hot cores similar to the models by Hassel et al. (2008), with $n = 2 \times 10^5$ cm^{-3} and $A_V = 10$ yield an abundance of $4-6 \times 10^{-8}$.

Based on absorption studies of C_3 in optical wavelengths the C_3 column densities in diffuse and translucent clouds are found to range between $10^{12}-10^{13}$ cm^{-2} (Maier et al. 2001; Roueff et al. 2002; Oka et al. 2003). The C_3 column density observed in the present study is larger by about a factor of 100 or more than those from the optical studies. Thus, the non-detection of C_3 in the foreground diffuse gas in the direction of our sources is consistent with the sensitivity of our observations.

Acknowledgements. HIFI has been designed and built by a consortium of institutes and university departments from across Europe, Canada and the United States under the leadership of SRON Netherlands Institute for Space Research, Groningen, The Netherlands and with major contributions from Germany, France and the US. Consortium members are: Canada: CSA, U. Waterloo; France: CESR, LAB, LERMA, IRAM; Germany: KOSMA, MPIfR, MPS; Ireland, NUI Maynooth; Italy: ASI, IFSI-INAF, Osservatorio Astrofisico di Arcetri-INAF; Netherlands: SRON, TUD; Poland: CAMK, CBK; Spain: Observatorio Astronómico Nacional (IGN), Centro de Astrobiologá (CSIC-INTA). Sweden: Chalmers University of Technology – MC2, RSS & GARD; Onsala Space Observatory; Swedish National Space Board, Stockholm University – Stockholm Observatory; Switzerland: ETH Zurich, FHNW; USA: Caltech, JPL, NHSC. J.C. and J.R.G. thanks spanish MICINN for funding support under projects AYA2009-07304 and CSD2009-00038. M.S. acknowledge support from grant N 203 393334 from Polish MNiSW.

References

Bieging, J. H., Wilson, T. L., & Downes, D. 1982, A&AS, 49, 607
Cernicharo, J., Goicoechea, J. R., & Caux, E. 2000, ApJ, 534, L199
Cohen, N. L., & Willson, R. F. 1981, A&A, 96, 230
Corbel, S., & Eikenberry, S. S. 2004, A&A, 419, 191
de Graauw, Th., Helmich, F. P., Phillips, T. G., et al. 2010, A&A, 518, L6
Falgarone, E., Phillips, T. G., & Pearson, J. C. 2005, ApJ, 634, L149
Fish, V. L., Reid, M. J., Wilner, D. J., & Churchwell, E. 2003, ApJ, 587, 701
Gendriesch, R., Pehl, T. F., Winnewisser, G., et al. 2003, Zeit. Naturforsch., 58a, 129
Gerin, M., De Luca, M., Black, J., et al. 2010, A&A, 518, L110
Giesen, T. F., Van Orden, A. O., Cruzan, J. D., et al. 2001, ApJ, 551, L181
Greaves, J. S., & Williams, P. G. 1994, A&A, 290, 259
Gwinn, C. R., Moran, J. M., & Reid, M. J. 1992, ApJ, 393, 149
Haffner, L. M., & Meyer, D. M. 1995, ApJ, 453, 450
Harvey, P. M., Campbell, M. F., & Hoffmann, W. F. 1977, ApJ, 211, 786
Hassel, G. E., Herbst, E., & Garrod, R. T. 2008, ApJ, 681, 1385
Herbst, E. 2005, ESA Special Publication, 577, 205
Hinkle, K. W., Keady, J. J., & Bernath, P. F. 1988, Science, 241, 1319
Jensen, P., Rohlfing, C. M., & Almloef, J. 1992, J. Chem. Phys., 97, 3399
Keene, J., Lis, D. C., Phillips, T. G., et al. 1999, The Universe as Seen by ISO, 427, 687
Lucas, R., & Liszt, H. S. 2000, A&A, 355, 327
Maier, J. P., Lakin, N. M., Walker, G. A. H., et al. 2001, ApJ, 553, 267
Miettinen, O., Harju, J., Haikala, L. K., & Pomrén, C. 2006, A&A, 460, 721
Mueller, K. E., Shirley, Y. L., Evans, N. J., II, et al. 2002, ApJS, 143, 469
Müller, H. S. P., Schlöder, F., Stutzki, J., & Winnewisser, G. 2005, J. Mol. Struct., 742, 215
Mufson, S. L., & Liszt, H. S. 1977, ApJ, 212, 664
Neufeld, D. A., Sonnentrucker, P., Phillips, T. G., et al. 2010, A&A, 518, L108
Nyman, L.-A. 1983, A&A, 120, 307
Oka, T., Thorburn, J. A., McCall, B. J., et al. 2003, ApJ, 582, 823
Ott, S. 2010, in Astronomical Data analysis Software and Systems XIX, ed. Y. Mizumoto, K. I. Morita, & M. Ohishi, ASP Conf. Ser., in press
Pety, J., Teyssier, D., Fossé, D., Gerin, M., et al. 2005, A&A, 435, 885
Pilbratt, G. L., Riedinger, J. R., Passvogel, T., et al. 2010, A&A, 518, L1
Plume, R., Kaufman, M. J., Neufeld, D. A., et al. 2004, ApJ, 605, 247
Roueff, E., Felenbok, P., Black, J. H., & Gry, C. 2002, A&A, 384, 629
Schmuttenmaer, C. A., Cohen, R. C., Pugliano, N., Heath, J. R., & Cooksy, A. L. 1990, Science, 249, 897
Van Orden, A., Cruzan, J. D., Provencal, R. A., et al. 1995, in Proc. Airborne Astronomy Symp. on the Galactic Ecosystem, ed. M. R. Haas, J. A. Davidson, & E. F. Erickson (San Francisco: ASP), ASP Conf. Ser., 73, 67
Vastel, C., Caux, E., Ceccarelli, C., et al. 2000, A&A, 357, 994
Ward-Thompson, D., & Robson, E. I. 1990, MNRAS, 244, 458
Wright, E. L., Fazio, G. G., & Low, F. J. 1977, ApJ, 217, 724

Appendix A: Formulae used for the excitation analysis

In the approximation of weak absorption ($\tau \ll 1$) and a negligible population in the upper, $v_2 = 1$, state, the lower state column density is given by:

$$N_l = \frac{8\pi\nu^3}{c^3}\frac{g_l}{A_{ul}\,g_u}\int \tau \mathrm{d}v \tag{A.1}$$

The rotational temperature, $T_{\rm rot}$, is calculated from the state specific column densities by

$$T_{\rm rot}(J, J') = \frac{E_J - E_{J'}}{k}\left[\ln\left(\frac{N_{J'}/(2J'+1)}{N_J/(2J+1)}\right)\right]^{-1} \tag{A.2}$$

where the energy of the levels is given by $E_J = hBJ(J+1)$ and the rotational constant for the lower vibrational state ($v_2 = 0$) is $B = 12\,908.242$ MHz.

Note that a ratio of level populations close to unity, $\left(\frac{N_{J'}/(2J'+1)}{N_J/(2J+1)}\right) \approx 1$, implies high values of $T_{\rm rot}$ in comparison to the rotational energy scale defined by $hB/k_{\rm B}$, i.e. 0.62 K in the case of C_3. The formal errors derived for the $T_{\rm rot}$ are correspondingly very large.

Assuming a thermalized population across the rotational ladder with a unique value of $T_{\rm rot}$ for all levels, a measured single state column density can be converted to the total column density $N(C_3)$ using:

$$N_{C_3} = P(T_{\rm rot})\,\frac{N_J}{2J+1}\,\exp\left(\frac{hB}{k_{\rm B}T_{\rm rot}}J(J+1)\right) \tag{A.3}$$

$$\approx \frac{T_{\rm rot}}{2hB/k_{\rm B}}\,\frac{N_J}{2J+1}\,\exp\left(\frac{hB}{k_{\rm B}T_{\rm rot}}J(J+1)\right) \tag{A.4}$$

where the approximation $T_{\rm rot} \gg hB/k$ has been applied for the partition function

$$P(T_{\rm rot}) = \sum_{J=0,2,4,\ldots}(2J+1)\exp\left(-E_J/kT_{\rm rot}\right) \approx \frac{k_{\rm B}T_{\rm rot}}{2hB}, \tag{A.5}$$

which is half of the usual value for a linear rotor due to the symmetry not allowing odd-J states.

[1] Tata Institute of Fundamental Research, Homi Bhabha Road, Mumbai 400005, India
e-mail: bhaswati@tifr.res.in
[2] I. Physikalisches Institut, University of Cologne, Germany
[3] Centro de Astrobiología, CSIC-INTA, 28850, Madrid, Spain
[4] LERMA, CNRS, Observatoire de Paris and ENS, France
[5] California Institute of Technology, Pasadena, CA 91125, USA
[6] JPL, California Institute of Technology, Pasadena, USA
[7] Onsala Space Observatory, Chalmers University of Technology, 43992 Onsala, Sweden
[8] Depts. of Physics, Astronomy & Chemistry, Ohio State Univ., USA
[9] The Johns Hopkins University, Baltimore, MD 21218, USA
[10] Institut d'Astrophysique Spatiale (IAS), Orsay, France
[11] Laboratoire d'Astrophysique de Marseille (LAM), France
[12] Laboratoire d'Astrophysique de Grenoble, France
[13] Université Toulouse; UPS; CESR; and CNRS; UMR5187, 9 avenue du colonel Roche, 31028 Toulouse Cedex 4, France
[14] Gemini telescope, Hilo, Hawaii, USA
[15] MPI für Radioastronomie, Bonn, Germany
[16] Institute of Physical Chemistry, PAS, Warsaw, Poland
[17] Nicolaus Copernicus University, Toruń, Poland
[18] Dept. of Physics & Astronomy, University of Calgary, Canada
[19] Nicolaus Copernicus Astronomical Center (CMAK), Toruń, Poland
[20] European Space Astronomy Centre, ESA, Madrid, Spain
[21] Infrared Processing and Analysis Center, California Institute of Technology, MS 100-22, Pasadena, CA 91125, USA
[22] Sterrewacht Leiden, University of Leiden, Leiden, The Netherlands
[23] SRON Netherlands Institute for Space Research, Landleven 12, 9747 AD Groningen, The Netherlands